An Interactive Simulator for Imposing Virtual Musculoskeletal Dynamics

Christopher J. Hasson

Abstract*—*Objective: **disease processes are often marked by both neural and muscular changes that alter movement control and execution, but these adaptations are difficult to tease apart because they occur simultaneously. This is addressed by swapping an individual's limb dynamics with a neurally controlled facsimile using an interactive musculoskeletal simulator (IMS) that allows controlled modifications of musculoskeletal dynamics. This paper details the design and operation of the IMS, quantifies and describes human adaptation to the IMS, and determines whether the IMS allows users to move naturally, a prerequisite for manipulation experiments.** ***Methods:*** **healthy volunteers (n = 4) practiced a swift goal-directed task (back-and-forth elbow flexion/extension) for 90 trials with the IMS off (normal dynamics) and 240 trials with the IMS on, i.e., the actions of a user's personalized electromyography-driven musculoskeletal model are robotically imposed back onto the user.** ***Results:*** **after practicing with the IMS on, subjects could complete the task with end-point errors of 1.56°, close to the speed-matched IMS-off error of 0.57°. Muscle activity, joint torque, and arm kinematics for IMS-on and -off conditions were well matched for three subjects (root-mean-squared error [RMSE] = 0.16 N·m), but the error was higher for one subject with a small stature (RMSE = 0.25 N·m).** ***Conclusion:*** **a well-matched musculoskeletal model allowed IMS users to perform a goal-directed task nearly as well as when the IMS was not active.** ***Significance:*** **this advancement permits real-time manipulations of musculoskeletal dynamics, which could increase our understanding of muscular and neural co-adaptations to injury, disease, disuse, and aging.**

***Index Terms*—Biomechanics, model personalization, motor learning, musculoskeletal modeling, myoelectric interface, robotics, sensorimotor control.**

I. Introduction

UNDERSTANDING how the nervous system learns and adapts to physiological modifications is critical for rehabilitation. The dynamical properties of key biological components such as muscle and tendon can be altered by injury, disease, disuse, and aging, changing how neural commands are converted to forces, joint torques, and ultimately limb motion.

Neural control strategies must adapt to musculoskeletal alterations to maintain motor function. However, it is difficult to pin down cause and effect relations because any singular physiological modification is likely accompanied by numerous other bodily changes and compensations, some of which are not readily observable. For example, experiments show that prolonged bed rest not only decreases strength but alters the force-velocity [1] and stiffness properties of muscle [2] as well.

To tease apart the effects of simultaneous neuromuscular modifications, independent and controlled manipulations are needed. One approach is to apply external forces to alter body dynamics, e.g., make a limb feel heavier or impose a novel force field. Such studies have shown that humans develop internal representations of limb dynamics to predict the effect of neural commands on limb action, and vice-versa [3], [4].

Less is known about how the neuromuscular system adapts to modifications of its internal dynamics, i.e., the path from neural excitation to muscular force and torque. Injury, disease, disuse, and aging can alter this path, which is difficult to access by direct manipulation. An alternative is to trick the nervous system into thinking the body's internal dynamics have been modified. This could be accomplished if an individual's neural commands were intercepted and routed through a musculoskeletal model, and sensory feedback provided to make it seem like the model was the individual's own body.

The present study takes the first step towards performing this trick by developing an interactive musculoskeletal simulator (IMS). In the IMS, a user controls a muscle activity-driven model of his or her arm, and a robotic interface makes the user's real arm follow the movement of the virtual arm. The distinguishing feature of the IMS is that it forcibly imposes the virtual arm's dynamics on the user; therefore, if the intrinsic musculoskeletal dynamics of the virtual arm are modified the user feels like his or her real arm dynamics are modified.

Existing myoelectric exoskeletons, while sharing some of the IMS design features, typically operate in a supporting role as torque amplifiers, and are designed to avoid hindering natural motion, i.e., to be transparent [5]–[8]. This is commonly achieved by minimizing resistive torques generated when electric motors are back-driven and compensating for the effects of exoskeleton weight and inertia. On the other hand, the IMS is intended to be non-back-drivable. Transparency is instead determined by the match between a user's real arm dynamics and the modeled dynamics. A close match produces high transparency, while purposeful alteration of the virtual arm properties reduces transparency in a way that mimics how the manipulation would feel if it could be performed on the user's real physiology.

Manuscript received February 2, 2017; revised March 22, 2017; accepted May 2, 2017. Date of publication May 10, 2017; date of current version February 16, 2018.

The author is with the Departments of Physical Therapy, Movement and Rehabilitation Sciences, Bioengineering, and Biology, Northeastern University, Boston, MA 02115 USA (e-mail: c.hasson@northeastern.edu).

Digital Object Identifier 10.1109/TBME.2017.2703298

The IMS builds upon prior work using electromyography (EMG)-driven virtual arms to predict muscle forces and joint torques, e.g., [9]–[11], and to test human motor control and learning hypotheses, e.g., [12], [13]. A key consideration is that in these studies, the user's arm is maintained in a fixed position to limit EMG movement artifacts. However, this curtails the role of proprioceptive feedback in virtual arm control, and may be a major reason task performance with EMG-driven virtual arms remains far below the actual limb. Forcing the real limb to follow the virtual limb, as done by the IMS, may improve task performance by bringing proprioceptive information back into the control loop, potentially outweighing the negative effects of EMG movement artifacts on virtual arm control.

During IMS operation, it is important that the forces users feel are due to the imposed musculoskeletal dynamics, rather than musculoskeletal model inaccuracies. If the model is well-matched to a user, the IMS becomes transparent, and in this case, the user should control the virtual arm as if it was his/her own. Once transparency is achieved, the virtual arm model can be deliberately altered to aid our understanding of how humans adapt to musculoskeletal modifications from neuromuscular disorders, disease states, and changes in physical activity.

Thus, the aims of this paper are to: 1) detail the design and operation of the IMS, 2) assess how users adapt to the IMS, and 3) evaluate whether a simple model personalization process and short IMS training session allows IMS users to move naturally, assessed by comparing muscle activation patterns, movement kinematics, and joint kinetics between IMS on and off states. A well-matched musculoskeletal model should promote high IMS transparency, improving confidence that adaptations to virtual musculoskeletal manipulations reflect reality.

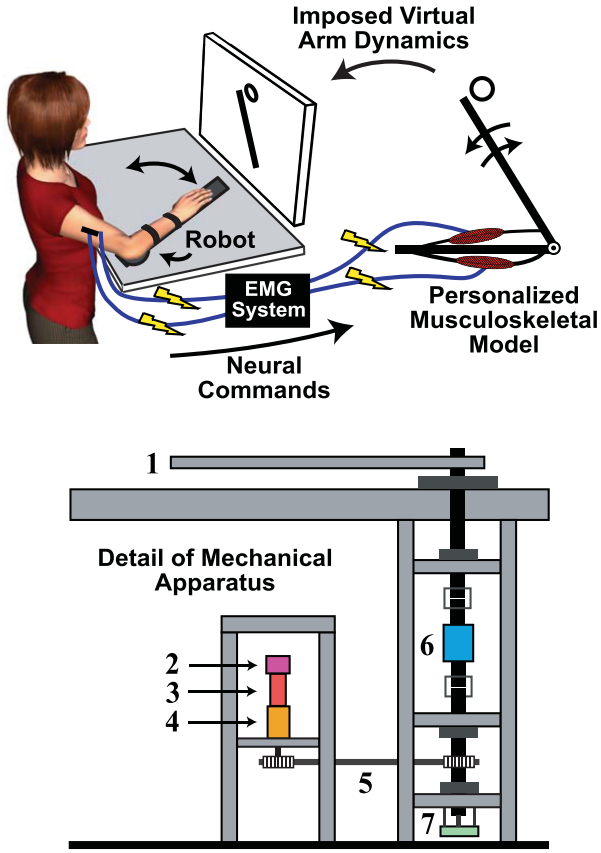

Fig. 1. Interactive musculoskeletal simulator (IMS). Top: EMG (electromyography) system, musculoskeletal model, and robotic interface. Bottom: Lever arm (1), motor encoder (2), DC motor (3), planetary gearhead (4), timing belt and pulleys (5), rotary torque sensor (6), and shaft encoder (7).

II. Interactive Musculoskeletal Simulator (IMS)

A. Overview

The IMS is comprised of three components (see Fig. 1): an electromyography (EMG) system to measure a user's muscle activity, a personalized musculoskeletal model controlled by the muscle activity, and a robotic device that forces the user's arm to match the musculoskeletal model's motion. In designing the IMS, each of the four musculoskeletal modeling design principles outlined by Winters [14] were considered as follows:

1) *A model is only as good as its weakest link.* One of the IMS components with the largest potential for introducing uncertainty during IMS operation is the surface-recorded EMG, which is contaminated by noise. Such errors can be reduced by measuring from muscles that are both large and superficial, maximizing signal-to-noise ratios. For this reason, EMG was sampled from the biceps and triceps brachii; other muscles, such as the brachioradialis, brachialis, and anconeus were not used for IMS control, as these muscles are typically smaller and/or less superficial. The trade-off for using a reduced set of muscles is that the experimental task must be constrained, in this case to a single degree-of-freedom planar rotation, to prevent changes in force-sharing among synergistic muscles.

2) *The modeling approach and degree of simplification should depend on the research question and motor task.* The purpose of the IMS is to simulate the dynamical behavior of a user's musculoskeletal system in real-time. The IMS modeling approach does not aim for anatomical accuracy, but instead strives for functional accuracy, i.e., representing the dynamic behavior of human muscle and tendon. The three principle requirements were that the IMS should allow users to: 1) quickly adapt to the system, 2) achieve a high level of motor performance, and 3) experience real-time virtual manipulations of musculoskeletal dynamics. To meet these requirements, a single degree-of-freedom rigid body skeletal model was used with lumped elbow flexor and extensor muscle models. The advantages of using lumped muscle models, instead of modeling each muscle independently, are threefold: 1) a simple mapping between real and virtual arm control (i.e., one real flexor muscle controls one virtual flexor muscle; likewise, for extensors), 2) a reduction in the number of model parameters, and 3) simplification of model personalization by eliminating synergistic muscle redundancy. Using lumped muscle models emulates changes typically affecting groups of muscles, such as aging [15]. The disadvantage of lumped muscle models is

that it precludes investigation of adaptation to changes in synergistic muscular dynamics. However, this can be addressed by adding more muscle models, which may also require more EMG channels and personalization procedures for proper functioning.

3) *The importance of model parameters is task-specific.* Even the simplest phenomenological musculoskeletal model has many parameters that must be specified. Pilot testing showed that the maximal isometric strength of the virtual arm model is a key parameter: if not well-matched to a user it was immediately noticeable. Thus, the virtual arm strength (and indirectly, muscle moment arms) were personalized for each subject. Clearly, other model parameters, especially the muscle properties, also influence model behavior [11], [16]. However, the aim of this study was to evaluate IMS performance in healthy users with just the basic strength personalization alone. Nevertheless, to model a specific neuromuscular injury, other properties may need personalization, and model accuracy could be increased where needed, for example by using ultrasound to measure and personalize muscle series-elastic stiffness [15].
4) *The use of musculoskeletal models to study and understand human movement usually requires optimization techniques.* Optimization is commonly used to solve the problem of force sharing among muscles [14]. Because the present model is EMG-driven, this was unnecessary, and optimization was instead used to personalize the model's strength.

B. Electromyography (EMG)

A wired EMG system monitored biceps and triceps (lateral head) muscle activity via bipolar parallel-bar silver surface electrodes (10 mm x 1 mm; 10 mm inter-electrode distance; Delsys, Natick, MA). Electrodes were placed on the skin near the center of the muscle bellies, orientated parallel with the underlying muscle fibers. Muscle activity was pre-amplified 10 x at the recording site and amplified again downstream for an overall amplification of either 1,000 or 10,000 (Bagnoli; Delsys, Natick, MA). The lower gain was used for subjects with large muscles and minimal subcutaneous adipose tissue. Amplified and band-pass filtered (from 20 $\pm$ 5 Hz to 450 $\pm$ 55 Hz; 80 dB/decade) biceps and triceps EMG signals were rectified and integrated using analog leaky integrators (NL703, Digitimer, Hertfordshire, United Kingdom) with time constants of 50 ms (similar to a first-order low-pass Butterworth filter with a cut-off frequency of about 3 Hz). Pilot testing showed that 50 ms was the longest time constant that did not produce a perceptible lag during IMS operation. The rectified and integrated EMG is denoted as iEMG, and henceforth will be used to approximate neural commands issued to the biceps and triceps muscles. For reference, the median frequency of the biceps and triceps iEMG power spectrum was 0.60 $\pm$ 0.12 Hz (mean $\pm$ one std. dev.) and 0.54 $\pm$ 0.14 Hz, respectively, for the four subjects in this study. Analog leaky integrators were used so the virtual arm simulation could run at a relatively low rate (100 Hz), and the iEMG could be sampled without aliasing (at 100 Hz). The iEMG signals were digitized with an 18-bit data acquisition board (PCI-6289, National Instruments, Austin, TX, USA) and served as inputs to the musculoskeletal arm model.

C. Musculoskeletal Arm Model

The lower arm was modeled as a rigid segment that rotated about a hinge joint in the horizontal plane (see Fig. 1), actuated by a pair of antagonistic lumped Hill-type muscle models [17], [18]. The flexor muscle model was controlled by biceps iEMG, and the extensor by triceps (lateral head) iEMG. Each muscle model contained a contractile element CE and series elastic element SEE (see Fig. 2; upper-left), with dynamics governed by two first-order differential equations: one specified CE activation dynamics (see [19, eq. (4)]) and another specified CE contraction dynamics (see [15, Appendix]). The force produced by each muscle model depended on four variables:

1) *CE Activation Level*. The CE became active in response to changes in iEMG, according to a first-order process with activation and deactivation time constants of 11 and 68 ms, respectively [19]. The activation dynamics mimicked processes associated with the release and reuptake of calcium in the neuromuscular junction and ranged from 0 to 1 (full activation).
2) *CE Length*. There was an optimal length L_0 at which the CE produced maximal isometric force P_0, with force capability dropping off at shorter or longer lengths per a parabolic force-length relation (54–146% L_0).
3) *CE Velocity*. The CE produced less force when shortening and more when lengthening according to a rectangular-hyperbola defining a force-velocity relationship. The force-velocity relation used normalized Hill coefficients a/P_0 (0.25) and b/L_0 (2.53 s^{-1}) and an eccentric plateau at 1.8 P_0.
4) *SEE Stiffness.* The SEE stiffness affects CE length and velocity. A compliant SEE will allow the CE to shorten more, and vice-versa. SEE stiffness was defined by a second-order polynomial with coefficients α (0.26) and β (52.3).

Values for L_0, series-elastic element slack length L_S, musculotendon length L_{MT}, and moment arm magnitude L_{MA} were based on the Stanford VA Upper Limb model [20] in OpenSim [21]. L_{MT} and L_{MA} were defined as continuous functions of the virtual arm angle θ_V, based on polynomials fit to the OpenSim model data. Since lumped muscle models were used, values for L_0, L_S, and L_{MT} were based on representative muscle heads. The flexor model used biceps (short head) parameters ($L_0 = 0.132$ m; $L_S = 0.192$ m) and the extensor used triceps (lateral head) parameters ($L_0 = 0.114$ m; $L_S = 0.098$ m).

D. Robotic Interface

A custom apparatus was designed to apply torques to subjects' arms, imposing the virtual arm dynamics (see Fig. 1). The apparatus consisted of a thermoplastic cradle to hold the subject's arm, attached to an aluminum lever arm mounted on a shaft connected to a 150 W brushless DC motor (torque constant

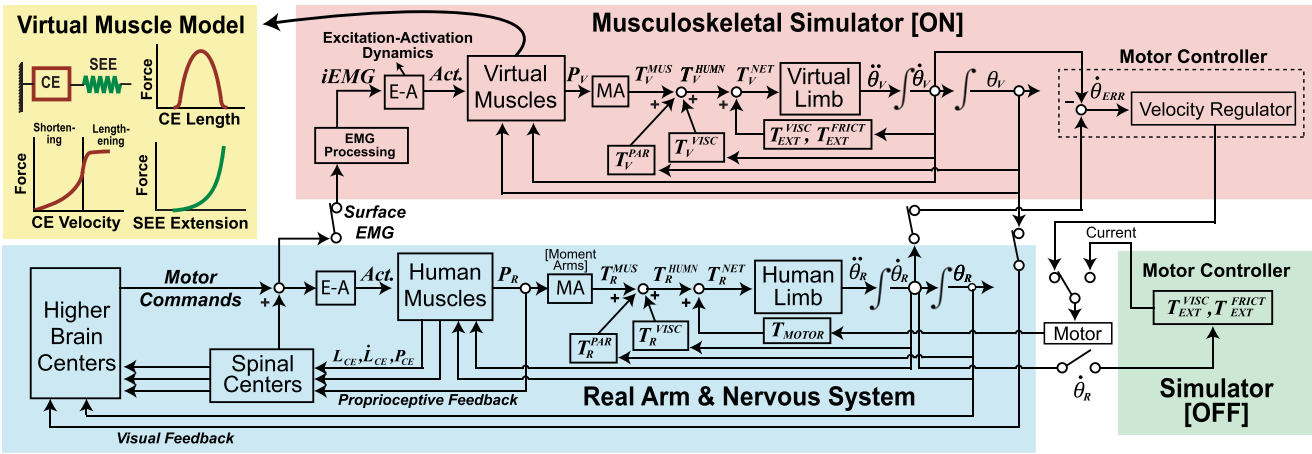

Fig. 2. Interactive musculoskeletal simulator (IMS) design. When the IMS is off, a user's real arm behaves normally, with motor-applied viscous T_{EXT}^{VISC} and frictional $T_{\mathrm{EXT}}^{\mathrm{FRICT}}$ torques to make task performance more challenging. Alternatively, when the IMS is on, the motor applies a torque T_{MOTOR} that forces a user's arm to follow the motion of a personalized virtual arm controlled by the user's muscle activity. With the IMS on, the real and virtual arms are controlled in parallel, and if the virtual arm dynamics match the real arm dynamics the user feels nothing unusual. If the virtual dynamics are purposefully modified, the user will feel like his/her real arm dynamics are modified. Variables θ, $\dot{\theta}$, and $\ddot{\theta}$ are angular arm position, velocity, and acceleration and P is muscular force. Torque T^{HUMN} is the total torque produce by the human body (real or virtual), which depends on the torque produced by the muscles T^{MUS} and from internally-generated parallel elastic and viscous torques, T^{PAR} and T^{VISC}, respectively. Variables in the virtual arm simulation have V for subscripts; those in the real world have R subscripts. The net torque T^{NET} is the sum of the human-generated torque T^{HUMN} and externally applied torques. Other variables: $L_{CE}, \dot{L}_{CE},$ and P_{CE} = muscle fiber length, velocity, and force, respectively; $\dot{\theta}_{ERR}$ = difference between the physical and virtual arm angular velocities. Note, real arm and nervous system are highly simplified.

= 36.3 mN·m/A; speed constant = 263 r/min/V; EC45; Maxon Motor AG) with an integrated angular position encoder (HEDL 9140; Maxon). Motor speed was reduced through a three-stage planetary gearhead (GP 52C; Maxon) with a 43:1 gear ratio, and then from a 20-tooth pulley mounted on the gearhead, through a timing belt, to a 30-tooth pulley on the shaft connected to the lever arm (a 1.5:1 gear ratio). The relatively high overall gear ratio was not a concern because IMS was designed to be non-back-drivable. The shaft was comprised of two sections with a rotary torque transducer (50 N·m capacity; resolution = 0.125 N·m; Model T8; Interface, Inc., Scottsdale, AZ) mounted between a lower shaft connected to the motor (via the pulley) and an upper shaft connected to the lever arm. Single-jointed shrink-disk hubs were used to couple the lower and upper shafts to the torque transducer. The shaft and lever arm angle was measured by an optical encoder (resolution = 0.045°; H3-8000-IE-D; US Digital, Vancouver, WA).

E. Simulator Operation

The IMS was operated in one of two ways (see Fig. 2). When turned off, the user's arm behaved normally, and the motor imposed an external viscous torque $T_{\mathrm{EXT}}^{\mathrm{VISC}}$ on the user's arm with a damping factor of -0.35 $\dot{\theta}_R$ to increase the task challenge, where $\dot{\theta}_R$ is the real arm angular velocity (subscript R denotes variables related to the real arm). For reference, this value is near the upper range of the values reported for intrinsic human elbow joint damping [22]. The presence of $T_{\mathrm{EXT}}^{\mathrm{VISC}}$ elevates the iEMG signal-to-noise ratio by increasing muscular effort (although effort remained low; typically, less than 20% of maximum). Because of the low-friction environment, $T_{\mathrm{EXT}}^{\mathrm{VISC}}$ was increased 2.5x to aid movement completion when the arm was within the target (±2.5° in accuracy-constrained condition and ±5° in speed-constrained condition). Between trials the motor brought the real arm back to the starting position.

With the IMS turned on, the virtual arm was controlled by the user's recorded biceps and triceps iEMG, and the motor moved the lever arm, and therefore the subject's arm, to match the angular velocity of the virtual arm $\dot{\theta}_V$ (subscript V denotes a virtual variable). The angular acceleration of the virtual arm $\ddot{\theta}_V$ was calculated by dividing the net virtual arm torque T_V^{NET} by its inertia I_V, with T_V^{NET} equal to the sum of two torques (see Fig. 2): 1) the internally generated torque T_V^{HUMN}, which depended on the torque produced by the virtual muscles T_V^{MUS}, a parallel elastic torque T_V^{PAR} (prevented the virtual arm from exceeding 20° beyond the starting position and waypoint), an internal viscous torque T_V^{VISC} (simulates intrinsic damping), and 2) the externally applied torques used to increase the task challenge, which included the external viscous torque $T_{\mathrm{EXT}}^{\mathrm{VISC}}$ matching the IMS-off condition, and a small frictional torque $T_{\mathrm{EXT}}^{\mathrm{VISC}}$ that approximated the small motor starting torque present in the IMS-off condition.

Each time new iEMG values were sampled, MATLAB's Runge-Kutta integration algorithm (ode23) was used to integrate the differential equations governing muscle model activation, contraction, and skeletal dynamics, to obtain updated virtual muscle activations, virtual muscle forces, and new virtual arm positions and velocities [23]. The position was used to update a visual display (XL2420G; BenQ, Costa Mesa, CA) showing the virtual arm and starting/waypoint graphics (see Fig. 3; lower right panel) via a high-performance video card (GeForce GTX 750 Ti; NVIDIA, Santa Clara, CA). The virtual arm velocity was sent from the MATLAB simulation program to a digital motor controller (EPOS2 50/5; Maxon) through a high-speed CAN interface (NI 9862; National Instruments).

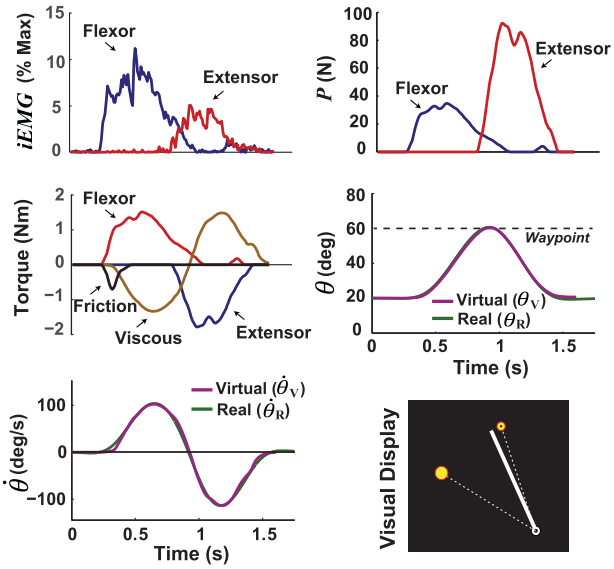

Fig. 3. Example of a trial with the musculoskeletal simulator turned on for one subject (subject S1). In response to excitation of the real biceps and triceps (*iEMG*), the virtual flexor and extensor muscles produced force (*P*) to move the virtual arm. A servomotor moved a physical lever arm containing subject's real arm to follow the virtual arm. The real (subscript R) and virtual (subscript V) arm angle θ and angular velocity $\dot{\theta}$ are shown. The lower right panel shows the visual feedback presented to subjects; the arm is shown just after leaving the starting position; the arm moved counterclockwise to a waypoint and back.

The EPOS2 controller adjusted the current supplied to the motor to make the physical arm velocity $\dot{\theta}_R$ match the virtual arm velocity $\dot{\theta}_V$ (see Fig. 2). Dual-loop regulation was used to control the motor and lever arm system, which compensated for the small amount of backlash ($\sim$1°) in the drive system. This regulation scheme consisted of an auxiliary controller that used motor velocity information to stabilize the control loop and a main controller that used the lever arm shaft velocity for speed regulation. Proportional-integrative (PI) control was used with velocity and acceleration feedforward compensation to adjust for friction and inertial loads. The controller gains were selected using automated tuning software (see EPOS2 documentation for more details). Target velocities were updated at 100 Hz, synchronized to the updating of the visual display.

An example of IMS operation with a human subject in the control loop (i.e., simulator on) is shown in Fig. 3. In this example, the virtual arm moved counter-clockwise from the starting position (20°) through a waypoint (60°), and back. Note the significance of the muscle properties: the extensor virtual muscle force is higher because the muscle is lengthening while active due to the CE force-velocity relation. As the virtual arm moved, the motor moved the subject's real arm to follow along. Comparing actual and virtual arm position and velocity time histories (see Fig. 3) shows that the real arm closely followed the virtual arm, with root-mean-squared positional errors of less than a degree. These errors, including the end-point error, are in part due to the accumulation of integration error during the forward dynamics simulation. The errors are small because the movements are relatively short (typically < 1.5 s), and the simulation was reset after each movement.

TABLE I
SUBJECT INFORMATION

Subject	S1	S2	S3	S4
Age (yrs)	36	29	26	26
Height (m)	1.88	1.56	1.68	1.80
Weight (kg)	77.2	53.1	69.9	65.5
Gender	M	F	F	M
Forearm Length[a] (m)	0.245	0.195	0.235	0.231
Hand Length[b] (m)	0.206	0.165	0.187	0.198
Arm Inertia[c] (kg·m^2)	0.069	0.027	0.051	0.052
Max. Flexor Torque (N·m)	51.2	29.4	38.2	48.6
Max. Extensor Torque (N·m)	44.2	31.5	26.3	39.2

[a]Elbow joint center to stylon.
[b]Wrist joint center to middle finger tip.
[c]Combined forearm and hand inertia about elbow flexion/extension axis.

F. Safety Considerations

The IMS is designed to impose virtual arm dynamics on a user, which means that anything that happens in the simulation happens to the user, within imposed limits. There were several redundant software and hardware controls in place to address potential safety issues. The servomotor controller position limits were set to be 5° beyond the virtual arm range of motion enforced by the parallel elasticity T_V^{PAR}, and mechanical stops were placed 5° beyond the servomotor position limits. The maximum $\dot{\theta}_R$ and $\ddot{\theta}_R$ were set to 500°/s and 48,000°/s^2, respectively. An emergency stop button that cut power to the motor was placed close to the user's left hand, which was free as only the right arm was restrained in the apparatus.

III. HUMAN SUBJECT TESTING

A. Subjects

Personalized virtual arm models were created for four healthy young subjects (see Table I), who practiced a goal-directed task with the IMS off (normal limb action) and on (imposed virtual arm dynamics). One of the subjects (S1) was experienced with the IMS (over 10 hours of practice); the others had no prior experience. Before participation, the purpose and risks of the study were explained to each subject, and they signed an informed consent document. The study was approved by the Northeastern University Institutional Review Board.

B. Task

The task consisted of a back-and-forth arm movement in the horizontal plane (see Fig. 1). Subjects were instructed to move their arm counterclockwise to pass through a waypoint and then back to the starting location, stopping their arm as close to a starting target circle center as possible (see Fig. 3, lower right). This task was chosen because it is representative of a wide class of everyday movements, e.g., bringing an object towards the body and putting it back. The starting position (20°) was at an elbow joint angle of 105° relative to the body (full elbow flexion = 0°; full extension = 180°). To reach the waypoint the elbow had to be flexed 40°. It did not matter how far past the

waypoint the arm moved, the waypoint only had to be passed. After starting the movement, the trial ended when the arm came to a stop (velocity $< 5°/s$; acceleration $< 20°/s^2$). If the arm did not pass the waypoint, a buzzer sounded after the trial was completed and the visual display indicated this failure.

C. Protocol

Stage 1 (Neural Excitation and Strength Scaling): By design, any strength mismatches between the real and virtual arms will be felt by the user. Therefore, a two-stage procedure was used to scale the iEMG and virtual muscle strength for each subject. In Stage 1, an initial "roughed-in" scaling was performed using maximal isometric muscular efforts. Subjects were seated next to a dynamometer (System 3 Pro; Biodex, Shirley, NY) with their torsos strapped to a chair and their right arm strapped to a metal bar attached to the dynamometer motor. The arm was fixed with the elbow joint center aligned with the dynamometer axis (the wrist was neutral). Subjects performed five maximal isometric contractions in the direction of elbow flexion and five in extension. For flexion the elbow was at 90° and for extension at 110° (full extension = 180°), approximately where maximal elbow torques are typically observed [24]. Each MVC lasted two seconds with a 30-second rest between trials. Torque was measured using the dynamometer's built-in torque sensor.

The average iEMG recorded during rest was used to establish measurement noise thresholds, defined as the mean resting iEMG plus three standard deviations. Only iEMG above this level excited the virtual muscles. The median of the five iEMG maximums recorded during the MVCs established 100% muscle excitation (iEMG ranged from 0–1). Similarly, the median of the maximum joint torques was divided by moment arms of 4.5 cm for the biceps (with elbow at 90°) and 2.0 cm for the triceps (with elbow at 110°), to customize the virtual bicep and triceps maximal isometric strengths (P_0) to the subject. These moment arms were derived from the OpenSim polynomials (see Section II-C). The virtual arm inertia was scaled to each subject using anthropometric measurements and models from de Leva [25].

Stage 2 (Practice with Simulator Off): Subjects performed the back-and-forth task with the simulator off for 50 trials with instructions to complete the movement in 1.2 s and stop within ±5° from the target center. Pilot experiments showed that this was a comfortable movement time for subjects.

Stage 3 (Neuromuscular Simulator Tuning): Although strength and anthropometric measures were used to personalize the musculoskeletal model to each subject in *Stage 1*, inaccuracies remain: 1) iEMG represents a limited tissue volume, 2) lumped and simplified muscle models were employed using several literature-based parameters, 3) maximal voluntary contractions are subject to error, and 4) muscle moment arms, which affect the relation between virtual muscle force output and joint torque, were not adjusted to each subject. Errors in any of these parameters will affect the "strength" of the virtual arm, e.g., if the muscle moment arms are too small the virtual arm will feel weak.

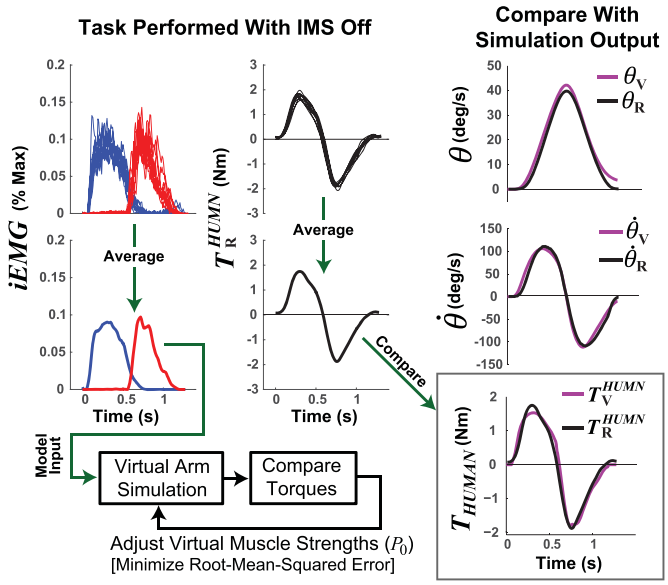

Fig. 4. Virtual arm model personalization. Representative muscle activity (iEMG) patterns measured during simulator-off task practice are used to perform a forward simulation of the virtual arm model. Virtual muscle strengths P_0 are tuned to make the virtual elbow torque T_V^{HUMN} match the measured torque from simulator-off practice T_R^{HUMN} (lower-right panel). The real and virtual (subscript R and V, respectively) arm angle θ and velocity $\dot{\theta}$ are shown.

A simple optimization procedure was used to correct these errors. The procedure used the scaled iEMG and joint torque data from the last 40 simulator-off practice trials of *Stage 1* (trials 11–50) to adjust the muscle P_0 values to best match the musculoskeletal model output to the real arm movement data. P_0 was chosen because it was one of the most sensitive parameters as shown by pilot work. Two adjustments were performed: 1) a global strength adjustment, which increased or decreased P_0 for both muscles by the same amount, and 2) a relative strength adjustment, which changed the ratio between the flexor and extensor muscle model P_0 values. While other musculoskeletal model parameters besides P_0 can have significant effects on musculoskeletal model behavior, such as L_0 and L_S [11], [16], this study aimed to adjust the fewest parameters possible. Muscle model origin-insertion lengths L_{MT} were not personalized and scaling these parameters did not have significant effects on the simulation output. Note that P_0 optimization indirectly adjusts for moment arm (L_{MA}) errors, e.g, if the flexor L_{MA} was too small for a subject, the personalization routine increases P_0 to compensate.

Of the 40 simulator-off trials used in the optimization, a subset with movement times within ±0.25 SD of the mean was selected, as illustrated in Fig. 4. Data from each trial in the subset was time-aligned to the start and end of movement (defined by the initial and final joint angular accelerations) and interpolated to 1000 evenly spaced points. These aligned trials were then averaged and smoothed to create representative iEMG and joint torque profiles (see Fig. 4).

An optimization routine (MATLAB function *fmincon.m*) adjusted the P_0 values to minimize the root-mean-square error (RMSE) between the virtual elbow torque T_V^{HUMN}, which was

calculated based on a forward dynamics simulation using the biceps and triceps iEMG as inputs, and the real human-generated elbow torque T_R^{HUMN} measured during the simulator-off trials, determined by

$$T_R^{\mathrm{HUMN}} = 0.5\left(T_R^{\mathrm{SEN}} + T_R^{\mathrm{NET}}\right)$$

where T_R^{SEN} is the torque measured by the rotary torque sensor, and T_R^{NET} is the net torque acting on the combined human and lever arm system, calculated from the arm + cradle moment of inertia I_R and angular acceleration $\ddot{\theta}_R$ ($T_R^{\mathrm{NET}} = I_R\ddot{\theta}_R$).

Each time the optimization changed P_0 a new forward simulation was performed and new RMSE computed, and this repeated until the changes in P_0 fell below 0.001. This took a few minutes and was repeated with different initial conditions to verify convergence. No timing parameters were adjusted, such as the CE activation/deactivation time constants, because the goal was to adjust the fewest number of parameters possible. Thus, there remained a small delay between the real and model-predicted torques. On average, the T_V^{HUMN} lagged T_R^{HUMN} by 37 ± 19 ms (mean ± one standard dev.) for the four subjects in this study, measured during simulator-on practice in *Stage 4* (see next paragraph). This delay was defined as the lag with the highest sample cross-correlation between T_V^{HUMN} and T_R^{HUMN} (MATLAB function *crosscorr.m*).

Stage 4 (Practice with Simulator On): After musculoskeletal model personalization, subjects practiced the task with the IMS on, i.e., their arm was forced to follow the movements of the iEMG-driven virtual arm. Two blocks of 40 speed-restricted trials were performed (80 total), followed by four blocks of 40 accuracy-restricted trials (160 total) with target diameter halved.

Stage 5 (Final Simulator-Off Practice): At the end of practice, subjects performed a second block of IMS-off trials. In addition to having restrictions on movement accuracy, subjects were instructed to move at a speed equal to the mean of the last 30 IMS-on trials to facilitate IMS off vs. on comparisons. This was because if subjects move faster in the IMS-off condition, muscle activity and joint torques will be elevated and temporally compressed.

D. Simulator Evaluation

Servomotor Performance: The degree to which the servomotor made the user's arm follow the virtual arm was quantified by the RMSE between virtual and measured arm angular displacement and velocity (θ_V vs. θ_R and $\dot{\theta}_V$ vs. $\dot{\theta}_R$).

Model Personalization: The quality of the musculoskeletal model personalization was assessed by the RMSE between the muscular torques produced during real arm movements and those simulated with the musculoskeletal model (T_R^{HUMN} vs. T_V^{HUMN}). Note, this comparison assesses the personalization process; how well the model predicts novel actions is quantified during human-in-the-loop (IMS-on) practice.

Task Skill: Movement time and accuracy defined task skill. If the personalized IMS models are reasonable representations of subjects' arm dynamics, then subjects should perform the task just as well with the IMS on vs. off.

Neuromuscular Adaptation and IMS Transparency: It is possible to compensate for an ill-fitted virtual arm model by altering neuromuscular control, but this would reduce transparency due to the mismatch between the real and virtual arm dynamics. Adaptation and transparency were assessed by comparing iEMG, human-generated torque, and movement kinematics for each IMS-on trial to the mean IMS-off pattern (mean of trials 290-330). If the virtual arm is a good representation of a subject's arm dynamics, these differences should be small, and any adaptations exhibited by the subjects would tend to decrease these differences. Since iEMG is always positive, the signed difference was computed, and the RMSE computed for the other variables because these have positive and negative values. Variables were normalized to the total trial movement time.

While the above analysis highlights trends during IMS-on practice, it is affected by trial-to-trial variations in movement time: a trial with a faster movement time will necessarily have greater iEMG and arm acceleration. To make the data sets more comparable, the last half of the accuracy-restricted IMS-on practice trials (n = 80) were sorted to isolate trials with movement times within one standard deviation of the mean end-of-practice IMS-off movement time. These were averaged and compared to the IMS-off average. Only the last half of data (80 of 160 trials) were used to avoid adaptation transients. Both the RMSE and R^2 between the representative speed-matched IMS-on and IMS-off trials was computed.

IV. Results

A. Servomotor Performance

When turned on the IMS made subjects' real arms closely follow the movements of their personalized virtual arms. The RMSE between the virtual arm position and velocity and that recorded by the shaft encoder (θ_V vs. θ_R and $\dot{\theta}_V$ vs. $\dot{\theta}_R$) was 0.84 ± 0.18° and 10.0 ± 3.2°/s, respectively (mean ± between-subjects standard dev.). An exemplar trial is shown in Fig. 3. Servomotor performance is aided by the relatively low frequency of human movement: the median normalized frequency of the $\dot{\theta}_V$ power spectrum was 0.76 ± 0.06 Hz (mean ± one between-subjects standard dev.) for the four subjects in this study, measured during simulator-on practice.

B. Model Personalization

The virtual elbow flexor and extensor muscle model strengths (P_0) were adjusted using an optimization routine that minimized the difference between the real muscular torque recorded during simulator-off practice trials (T_R^{HUMN}) and the torque predicted by feeding the same simulator-off iEMG through the virtual arm simulation (T_V^{HUMN}). The RMSE between the real and virtual torque, arm angle, and arm angular velocity was 0.16 ± 0.05 N·m, 2.5 ± 0.72°, and 15 ± 1.84°/s (mean ± between-subjects standard dev.), respectively (see Fig. 5).

C. Task Skill

Skill was defined by movement time and accuracy. High skill is reflected by fast and accurate movements. If the virtual arm

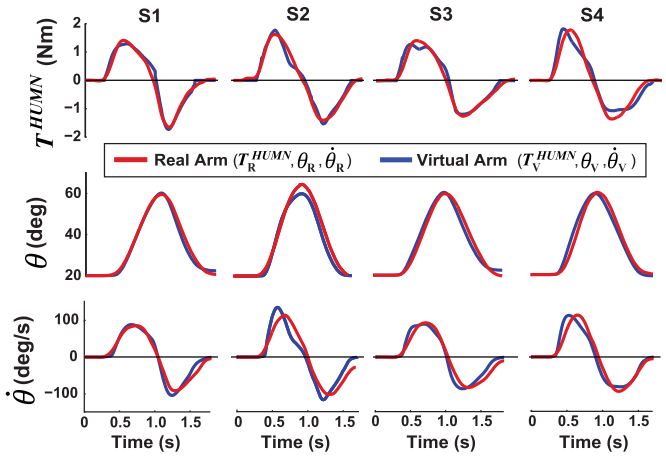

Fig. 5. Results of interactive musculoskeletal simulator (IMS) personalization showing that the simulated virtual arm model output (blue lines) was generally well-matched to each subject's real arm performance (red lines).

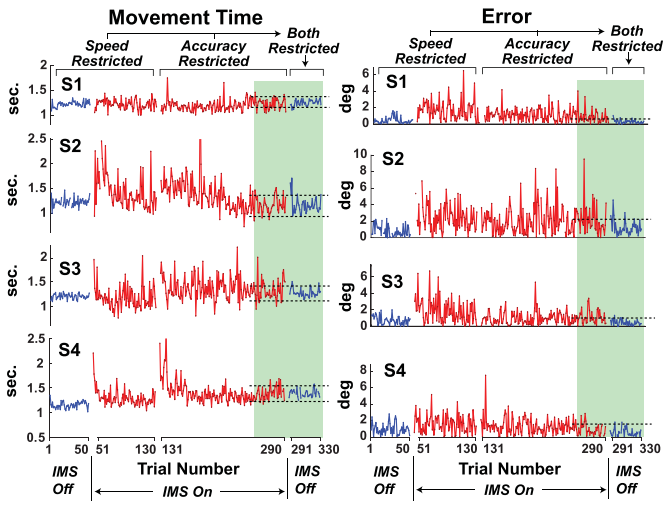

Fig. 6. As subjects practiced controlling the virtual arm with the interactive musculoskeletal simulator (IMS) turned on, movement time and endpoint error approached the simulator-off condition. The simulator was off at the start of practice (blue), on for the next 240 trials (red), and was then off again at the end of practice (blue).

is well-personalized, then IMS-on task skill should be similar to IMS-off skill. With the IMS off, subjects easily moved in the 1.2 s comfortable-speed target time, with a mean movement time of 1.21 ± 0.04 s and an average error of 1.0 ± 0.6° for the last 30 trials of the initial speed-restricted practice block (trials 1–50; Fig. 6). When the IMS was first turned on, subjects showed an increase in movement time and/or decreased accuracy, and trial-to-trial variability increased (see Fig. 6). After practicing with the IMS on under speed-restricted conditions, subjects were able to decrease their movement time, approaching the 1.2 s target time (1.24 ± 0.05 s). However, the angular error remained higher (1.7 ± 0.4°; trials 101–130).

After 80 IMS-on practice trials, subjects were instructed to focus more on accuracy, and the target size was reduced by half. This caused movement time to increase for subjects

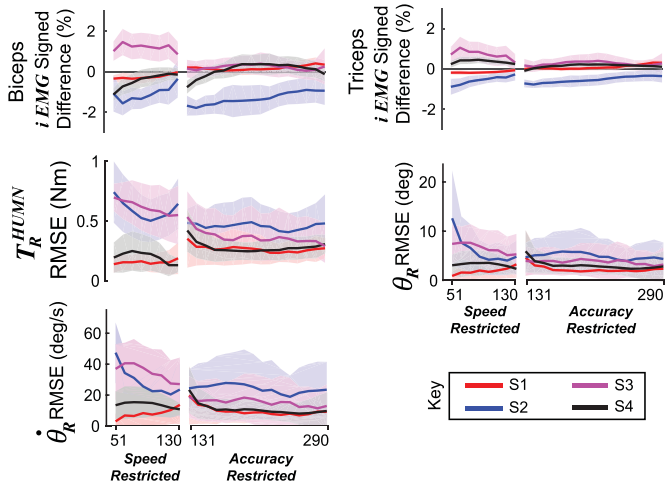

Fig. 7. Trial-by-trial differences between muscle activity (iEMG), and real joint torque (T_R^{HUMN}), joint angle (θ_R), and joint angular velocity ($\dot{\theta}_R$) patterns for interactive musculoskeletal simulator (IMS)-on trials compared with the mean IMS-off patterns (trials 290-330) for each of the four subjects. Note for iEMG the signed difference is shown; the root-mean-squared error (RMSE) is shown for the other variables. Trials were averaged in non-overlapping bins of 10 trials. Shading = standard deviation within each 10-trial bin.

S2-S4, but accuracy did not show a large change (see Fig. 6). With continued IMS-on practice, speed and accuracy approached, but did not equal the IMS-off condition. At the end of IMS-on practice (trials 261–290), movement time reduced to 1.27 ± 0.11 s and the average absolute angular end-point error was 1.6 ± 0.7°. Trial-to-trial variability remained higher with the IMS on (see Fig. 6). For the final IMS-off trials (trials 301–330), speed and accuracy were restricted to match the previous IMS-on trials as closely as possible. This restriction was enacted to facilitate IMS on vs. off comparisons (see next section). For these trials, movement time was 1.27 ± 0.09 s and end-point error was 0.6 ± 0.3° (mean ± between-subjects std. dev.; Fig. 6).

D. Neuromuscular Adaptation and IMS Transparency

IMS users could maintain speed and accuracy with an ill-fitting model by changing their control strategies. To evaluate subject adaptation to the IMS, the patterns of biceps and triceps iEMG, human-generated joint torque, and arm kinematics for each IMS-on trial were compared against the average IMS-off patterns. For three subjects, the biceps and triceps iEMG converged to the IMS-off patterns (see Fig. 7) but remained depressed for subject S2, which indicates a too-strong musculoskeletal model. Overall, differences were greater for biceps compared to triceps. For the other variables, the two female subjects (S2 & S3) had generally larger errors and converged more slowly than the males (S1 & S4).

While Fig. 7 makes trends visible, it does not provide a precise comparison because of the trial-to-trial variation in movement time, i.e., some trials are faster than others, and these require greater muscle activations, artificially increasing differences. This was addressed by sorting the last half of the accuracy-

TABLE II
ROOT-MEAN-SQUARED ERROR (RMSE) AND COEFFICIENT OF DETERMINATION (R^2) BETWEEN SPEED-MATCHED TASK PERFORMANCE WITH PERSONALIZED MUSCULOSKELETAL SIMULATOR ON VERSUS OFF

	Bi. *iEMG*		Tri. *iEMG*		T_R^{HUMN}		θ_R		$\dot{\theta}_R$	
Sub.	RMSE[a]	R^2	RMSE[a]	R^2	RMSE[b]	R^2	RMSE[c]	R^2	RMSE[d]	R^2
S1	0.44	.97	0.65	.81	0.14	.99	1.48	.99	5.72	.99
S2	2.66	.93	1.17	.77	0.25	.89	1.64	1.0	5.03	1.0
S3	0.83	.92	0.99	.89	0.21	.84	1.30	.99	4.56	.99
S4	1.00	.97	0.48	1.0	0.13	.98	1.87	.98	7.54	.97
Mean	1.23	.95	0.82	.78	0.18	.92	1.37	.99	5.21	.99
SD	0.98	.03	0.32	.08	0.06	.07	0.60	.01	2.06	.01

[a]Normalized (0–100%).
[b]N·m.
[c]deg.
[d]deg/s.

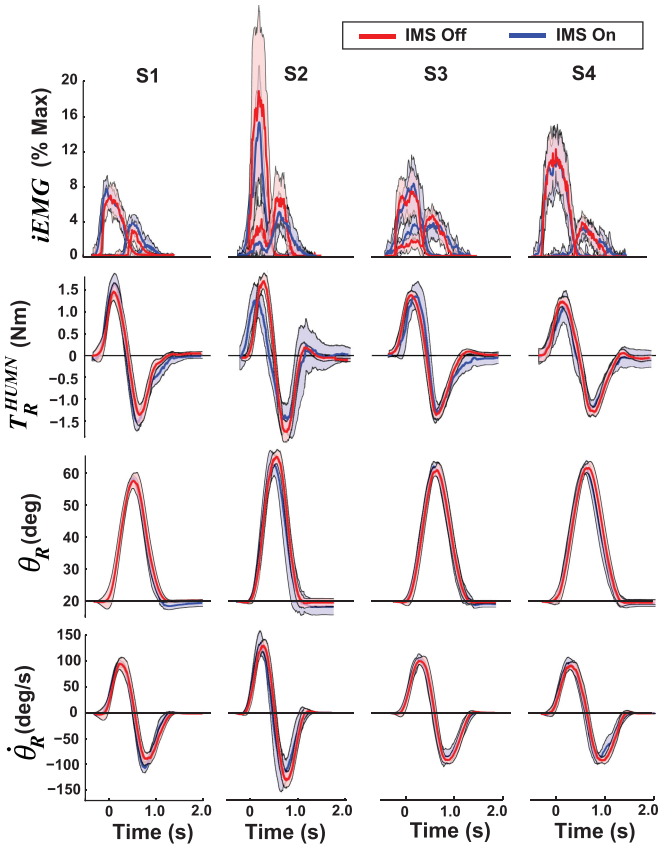

Fig. 8. For three out of four subjects (S1, S3, and S4), arm control with the interactive musculoskeletal simulator (IMS) on (blue lines) closely resembled arm control with the IMS off (red lines). The shading shows the standard deviation across trials.

restricted IMS-on practice trials (n = 80) to isolate those with movement times within one standard deviation of the mean end-of-practice IMS-off movement time. The differences between representative speed-matched IMS-on vs. -off patterns are presented in Table II and Fig. 8. The largest differences were again observed for subject S2, who had less muscle activation and muscular torque with the simulator on compared to off (the virtual arm was "stronger" than the actual arm).

V. DISCUSSION

A. Main Findings

An interactive musculoskeletal simulator (IMS) was developed to investigate how the neuromuscular system adapts to virtual modifications of its internal physical dynamics. This report detailed the design and operation of the IMS, assessed how users adapt to the IMS, and tested whether the IMS allows users to perform a goal-directed task as they naturally would—a prerequisite for manipulation experiments.

A brief model personalization routine followed by a short practice session allowed most subjects to become proficient at controlling their arm within the IMS, with skill approaching that of normal arm movements during comfortable-speed goal-directed actions. This level of skill is significant because making both fast and accurate movements with EMG-driven prostheses (both virtual and real) has proved challenging [26]. High proficiency was possible because with a well-matched musculoskeletal model, the virtual arm moves with the real arm and no unusual forces or torques are felt. The two arms (virtual and real) were well-matched for three out of four subjects by the end of practice, evidenced by similar muscle activity patterns, joint kinetics, and joint kinematics with the IMS off vs. on. A good match is critical because as shown, a well-matched model permits "natural" sensorimotor control, which should improve confidence that adaptations to virtual manipulations of musculoskeletal dynamics reflect reality.

B. Task Skill

The experimental task was a relatively fast goal-directed back-and-forth arm movement. While mechanically simple at the joint level, the task required precisely regulated and coordinated muscle activations. Unlike motors which are typically linear in their input-output behavior, muscles have nonlinear dynamics and force production depends on muscle length, velocity, and stiffness. Because of the displacement and speed of the arm, these dynamics came into play. For example, the flexor contractile element typically shortened by about 4 cm with a peak velocity of about 0.14 m/s $(1.0\,L_0/s)$. This produced a length-dependent reduction in force capability from $0.9\,P_0$ at rest $(90\%\,L_0)$ to $0.25\ P_0\,(55\%\,L_0)$ as the contractile element shortened and moved further on to the ascending limb of its force-length relation and a velocity-dependent reduction in force capability of $0.64\ P_0$ (at highest velocity). The extensor muscle model lengthened while active, and therefore produced more force than the flexor for a given excitation (e.g., Fig. 3), as it acted on the eccentric plateau of its force-velocity relation.

Despite this internal dynamical complexity, on average, subjects approached a level of skill (i.e., speed and accuracy) close to their real arm within one practice session. However, trial-to-trial variability remained higher with the IMS on, which may be due to small random errors induced by noise in the EMG signals. This variability is consistent with other reports [11] and current thinking on the limits of solely open-loop EMG-driven musculoskeletal model simulations [27]. Al-

though adding feedback loops to the model can compensate for noise-induced inaccuracies [28]; this would deflect from the main IMS capability—separating an individual's neural control system from the mechanics so the latter can be (virtually) modified. Layering additional neural dynamics on top of the real system, such as a modeled stretch reflex, may complicate interpretations of adaptations to biomechanical modifications (yet, could be interesting). Note, however, that the IMS is not purely open-loop, as the user physically interacts with the virtual arm, and therefore intrinsic reflexes remain involved.

How does subjects' skill compare to prior studies? The novelty of the present paradigm, i.e., physically imposing simulated virtual arm motion back onto the subject, means that there are few direct comparisons. The closest is a study by Johnson *et al*. [29], who showed that healthy subjects controlling a virtual prosthetic arm reached a mean absolute error of about 20° for a single point-to-point forearm rotation of about 180° with a movement time of 3 s. In contrast, subjects in the present study had end-point errors of about 1.5° and a faster 1.2 s movement time, albeit with a smaller range of motion (80° peak-to-peak). Subjects may have performed better in the present study because the arm was not restrained and thus proprioceptive feedback, which has a critical role in sensorimotor control [30], was not restricted.

C. Musculoskeletal Model Transparency

Because virtual arm dynamics were imposed on users, IMS transparency becomes a measure of the musculoskeletal model's accuracy. (Limitations associated with the hardware, such as the following error, will also affect transparency. However, as demonstrated, these are small.) If the virtual arm dynamics reasonably match each user's real arm dynamics, then users should feel as though they are controlling their own arms, because, in effect, they are (the apparatus just follows along). Virtual arm "feel" was quantified by muscle activation, joint torque, and movement kinematics. For most subjects, these measures were similar between IMS-on and -off conditions for speed-matched trials, showing high IMS transparency.

However, for subject S2 transparency was lower because the virtual arm was too strong, which could be related to anthropomorphic factors: subject S2 had a short stature, and many of the non-personalized model parameters were based on male anatomy via the OpenSim model. The transparency for subject S2 would likely be improved if more parameters besides P_0 were adjusted, but the aim of this study was to determine how well the IMS performed with a basic personalization process adjusting the fewest parameters possible. Note that although the moment arms were not personalized, optimization of P_0 values compensates for scaling errors in the moment arm vs. joint angle relation, i.e., if the moment arm was too large P_0 would be adjusted downwards. Thus, the source of error may stem from other unadjusted properties, such as the optimal CE length and SEE slack length, which can have non-negligible effects on the estimated muscle model force [11], [16].

Future work can and should explore the effects of adding muscles to the model; however, this causes the number of unknowns to increase exponentially, as each added muscle requires specification of several muscle dynamics parameters that require experimentation to personalize. Other parameters such as muscle lengths and moment arms could be scaled using anthropometric measures and modeling software (OpenSim).

D. Adaptation

Even for subjects in which the IMS model appeared to be well-matched, adaptation was not instantaneous, and it took some time to approach natural muscle activity, torque, and kinematic patterns. This raises the question, what are subjects adapting to? One explanation is that the nervous system learned to make adjustments to feed-forward motor commands and reflex gains to account for mismatches between the predicted and actual sensory feedback resulting from discrepancies in the real vs. modeled virtual arm dynamics [31], e.g., if the virtual arm is too strong, the real arm will move faster than expected, which may prompt a decrease in feed-forward commands and/or reflex gains. Increasing the model's anatomical realism could increase the adaptation rate, but this hypothesis is largely untested. One study compared the adaptation rate between individuals who learned to control an EMG-driven virtual arm with muscle models vs. one that had simpler force generators, but showed no differences [12]. In addition, the benefits of adding detail to a specific model component should be balanced against the potential financial and temporal costs associated with measuring and personalizing the component, and the effects of inaccuracies if the component is left unpersonalized.

E. Limitations

The IMS was made sufficiently complex to fulfill its design goal: to perform studies investigating how the neuromuscular system adapts to modifications of its internal dynamics. The simple design limits mechanical inaccuracies, reduces the number of unknown model parameters, and constrains available movement strategies. However, this also limits generalizability. It is not known how the results might change for more complex multi-joint movements. Further, the modeling approach aimed for functional, and not anatomical, accuracy by using lumped muscle models. If greater anatomical accuracy is needed to model a specific disorder, other musculoskeletal structures can be incorporated into the model, and finer-grained personalization procedures could be employed to adjust relevant model parameters, such as the force-velocity relation, series elastic stiffness, or muscle moment arms (e.g., see [15]).

VI. Conclusion

This paper presents an interactive musculoskeletal simulator (IMS), which consists of a personalized EMG-driven musculoskeletal model and robotic device that imposes the model's dynamics on the user. The results show that a well-matched musculoskeletal model allows IMS users to perform a goal-directed task nearly as well as when the IMS is not active, with similar neural control patterns, joint kinetics, and kinematics. This is significant, as achieving both speed and accuracy has been a

persistent challenge with EMG-driven prostheses (both virtual and real). This advancement permits real-time manipulations of musculoskeletal dynamics, which can be used to increase our understanding of muscular and neural co-adaptations to injury, disease, disuse, and aging.

Acknowledgment

The author thanks Sarah Goodman, Rachel Montenegro, and Michelle Wangrow for assistance with pilot studies.

References

[1] K. Funato *et al.*, "Changes in force-velocity and power output of upper and lower extremity musculature in young subjects following 20 days bed rest," *J. Gravit. Physiol.*, vol. 4, pp. S22–S30, 1997.

[2] K. Kubo *et al.*, "Changes in the elastic properties of tendon structures following 20 days bed-rest in humans," *Eur. J. Appl. Physiol.*, vol. 83, pp. 463–468, 2000.

[3] D. M. Wolpert *et al.*, "An internal model for sensorimotor integration," *Science*, vol. 269, pp. 1880–1882, 1995.

[4] M. Kawato *et al.*, "A hierarchical neural-network model for control and learning of voluntary movement," *Biol. Cybern.*, vol. 57, pp. 169–185, 1987.

[5] E. E. Cavallaro *et al.*, "Real-time myoprocessors for a neural controlled powered exoskeleton arm," *IEEE Trans. Biomed. Eng.*, vol. 53, no. 11, pp. 2387–2396, Nov. 2006.

[6] C. Fleischer and G. Hommel, "A human–exoskeleton interface utilizing electromyography," *IEEE Trans. Robot.*, vol. 24, no. 4, pp. 872–882, Aug. 2008.

[7] D. P. Ferris *et al.*, "An improved powered ankle–foot orthosis using proportional myoelectric control," *Gait Posture*, vol. 23, pp. 425–428, 2006.

[8] H. Kawamoto and Y. Sankai, "Comfortable power assist control method for walking aid by HAL-3," in *Proc. IEEE Int. Conf. Syst., Man, Cybern.*, vol. 4, 2002, p. 6.

[9] K. Manal *et al.*, "A real-time EMG-driven virtual arm," *Comput. Biol. Med.*, vol. 32, pp. 25–36, 2002.

[10] D. G. Lloyd and T. F. Besier, "An EMG-driven musculoskeletal model to estimate muscle forces and knee joint moments in vivo," *J. Biomech.*, vol. 36, pp. 765–776, 2003.

[11] J. W. Pau *et al.*, "Neuromuscular interfacing: Establishing an EMG-driven model for the human elbow joint," *IEEE Trans. Biomed. Eng.*, vol. 59, no. 9, pp. 2586–2593, Sep. 2012.

[12] C. J. Hasson, "Neural representation of muscle dynamics in voluntary movement control," *Exp. Brain Res.*, vol. 232, pp. 2105–2119, 2014.

[13] C. J. Hasson *et al.*, "Neural control adaptation to motor noise manipulation," *Front. Hum. Neurosci.*, vol. 10, 2016, doi: 10.3389/fnhum.2016.00059.

[14] J. M. Winters, "How detailed should muscle models be to understand multi-joint movement coordination?" *Hum. Movement Sci.*, vol. 14, pp. 401–442, 1995.

[15] C. J. Hasson and G. E. Caldwell, "Effects of age on mechanical properties of dorsiflexor and plantarflexor muscles," *Ann. Biomed. Eng.*, vol. 40, pp. 1088–1101, 2012.

[16] C. Y. Scovil and J. L. Ronsky, "Sensitivity of a Hill-based muscle model to perturbations in model parameters," *J. Biomech.*, vol. 39, pp. 2055–2063, 2006.

[17] A. Hill, "The heat of shortening and the dynamic constants of muscle," *Proc. R. Soc. Lond. B Biol. Sci.*, vol. 126, pp. 136–195, 1938.

[18] F. E. Zajac, "Muscle and tendon: Properties, models, scaling, and application to biomechanics and motor control," *Crit. Rev. Biomed. Eng.*, vol. 17, pp. 359–411, 1988.

[19] C. C. Raasch *et al.*, "Muscle coordination of maximum-speed pedaling," *J. Biomech.*, vol. 30, pp. 595–602, 1997.

[20] K. R. Holzbaur *et al.*, "A model of the upper extremity for simulating musculoskeletal surgery and analyzing neuromuscular control," *Ann. Biomed. Eng.*, vol. 33, pp. 829–840, 2005.

[21] S. L. Delp *et al.*, "OpenSim: Open-source software to create and analyze dynamic simulations of movement," *IEEE Trans. Biomed. Eng.*, vol. 54, no. 11, pp. 1940–1950, Nov. 2007.

[22] K. C. Hayes and H. Hatze, "Passive visco-elastic properties of the structures spanning the human elbow joint," *Eur. J. Appl. Physiol. Occupat. Physiol.*, vol. 37, pp. 265–274, 1977.

[23] E. K. Chadwick *et al.*, "A real-time, 3-D musculoskeletal model for dynamic simulation of arm movements," *IEEE Trans. Biomed. Eng.*, vol. 56, no. 4, pp. 941–948, Apr. 2009.

[24] Y. Kawakami *et al.*, "Specific tension of elbow flexor and extensor muscles based on magnetic resonance imaging," *Eur. J. Appl. Physiol. Occupat. Physiol.*, vol. 68, pp. 139–147, 1994.

[25] P. De Leva, "Adjustments to Zatsiorsky-Seluyanov's segment inertia parameters," *J. Biomech.*, vol. 29, pp. 1223–1230, 1996.

[26] J. Lobo-Prat *et al.*, "Non-invasive control interfaces for intention detection in active movement-assistive devices," *J. Neuroeng. Rehabil.*, vol. 11, 2014, doi: 10.1186/1743-0003-11-168.

[27] M. Sartori *et al.*, "Neural data-driven musculoskeletal modeling for personalized neurorehabilitation technologies," *IEEE Trans. Biomed. Eng.*, vol. 63, no. 5, pp. 879–893, May 2016.

[28] M. Sartori *et al.*, "Hybrid neuromusculoskeletal modeling to best track joint moments using a balance between muscle excitations derived from electromyograms and optimization," *J. Biomech.*, vol. 47, pp. 3613–3621, 2014.

[29] R. E. Johnson *et al.*, "The effect of powered prosthesis control signals on trial-by-trial adaptation to visual perturbations," in *Proc. IEEE Conf. Eng. Med. Biol. Soc.*, 2014, pp. 3512–3515.

[30] K. J. Kuchenbecker *et al.*, "Effects of visual and proprioceptive motion feedback on human control of targeted movement," in *Proc. IEEE Int. Conf. Rehabil. Robot.*, 2007, pp. 513–524.

[31] D. M. Wolpert *et al.*, "Perspectives and problems in motor learning," *Trends Cogn. Sci.*, vol. 5, pp. 487–494, 2001.